Compact Dual-Band Differential Bandpass Filter Using Quadruple-Mode Stepped-Impedance Square Ring Loaded Resonators

BAOPING REN[1,2] , **(Student Member, IEEE), HAIWEN LIU[3], (Senior Member, IEEE),**
ZHEWANG MA[1], (Member, IEEE), MASATAKA OHIRA[1], (Member, IEEE), PIN WEN[1,2],
XIAOLONG WANG[4], (Member, IEEE), AND XUEHUI GUAN[2], (Member, IEEE)

[1]Graduate School of Science and Engineering, Saitama University, Saitama 338-8570, Japan
[2]School of Information Engineering, East China Jiaotong University, Nanchang 330013, China
[3]School of Electronics and Information Engineering, Xi'an Jiaotong University, Xi'an 710049, China
[4]State Key Laboratory of Integrated Optoelectronics, Jilin University, Changchun 130012, China

Corresponding author: Haiwen Liu (haiwen_liu@hotmail.com)

ABSTRACT In this paper, a new quadruple-mode stepped-impedance square ring loaded resonator (SI-SRLR) is proposed, and a high-performance dual-band differential bandpass filter (BPF) is developed. Resonant characteristics of the SI-SRLR are investigated by the even-/odd-mode method and simulation techniques. Two differential-modes (DMs) of the SI-SRLR are used to form the dual differential passbands. The admittance ratio K of the SI-SRLR is chosen appropriately to prevent the common-mode (CM) interference with DM operations. Moreover, an open-circuited stub is added to enhance the CM suppression, while a source-load coupling is introduced to produce multiple transmission zeros and improve significantly the frequency selectivity of DM passbands. Finally, a dual-band differential BPF is designed, fabricated, and measured. Good agreement between the simulated and measured results verifies well the proposed structure and design method.

INDEX TERMS Differential bandpass filter, dual-band filter, quadruple-mode resonator, stepped-impedance square ring loaded resonator.

I. INTRODUCTION

Differential BPFs are widely used in modern communication systems for their good common-mode (CM) rejection capability, which results in higher immunity to the environmental noise and electromagnetic interference as compared with their single-ended counterparts [1]. So far, many differential BPFs have been developed by using coupled lines [2] or coupled resonators [3], [4]. For coupled-line based differential BPFs, all-stop type coupled-lines are often constructed in CM equivalent circuits to stop the CM transmission [2]. For differential BPFs using coupled- resonators, bi- and tri-section stepped-impedance resonators can provide enough freedom in obtaining differential-mode (DM) and CM characteristics of the BPFs [3], [4]. Although performing extremely well, these differential topologies are only suitable for single-band operations.

With the continuous appearance of various wireless equipments having multi-functional services, multi-band differential BPFs are highly desired. For dual-band operations with good in-band CM suppression, differential dual-band BPFs were introduced based on coupled stepped-impedance resonators (SIRs) [5]–[7] and center-loaded half-wavelength resonators [8]–[10]. To improve the CM suppression, extra additional terminating microstrip lines [5], [9], [10] or surface-mounted devices (SMDs) [6]–[8] were loaded to some of the resonators. By tuning the electrical lengths of open stubs or the values of lumped elements, the CM rejection level can be well optimized. Differential dual-band BPFs are developed by multimode resonators with inherent bandstop characteristics, such as the usage of the asymmetrical coupled-lines in [11], open/short-ended coupled SIRs in [12], multimode slotline resonators [13], [14] and modified

coupled-embedded resonators [15]. These designs have the advantage of good CM suppression without any additional loaded elements but need multi-layer process and complicated design. Some other novel methods have also been proposed to design differential dual-band BPFs, such as using doubly short-ended half-wavelength resonator in coupled-line structure [16], substrate integrated waveguide (SIW) technology [17], [18], varactor- and stub-loaded dumbbell-shaped resonator [19], or quad-mode stub-loaded twin-ring resonator [20]. Although good DM transmission are achieved in these reports, these designs suffer from large circuit sizes because of the cascaded multiple resonators or the CM suppression needs to be improved. In all, the study on differential dual-band BPFs is in progress, but still limited.

Recently, a quadruple-mode square ring loaded resonator (SRLR) is proposed for multi-band filter design [21]. All line widths of SRLR are assumed equal for analysis simplicity, resulting in a limitation of design freedom. To improve the design flexibility, an additional open stub loaded on the center of square ring in [22] or disperse technique used in [23] are conducted. Nevertheless, a favorable frequency disparity between two adjacent even-mode and odd-mode of the afore-presented resonators is not easy to achieve, which is disadvantaging to construct a differential filter with a desired CM suppression.

In this paper, a quadruple-mode stepped-impedance SRLR (SI-SRLR) is proposed, and a compact dual-band differential BPF is developed. The operating mechanism of the proposed SI-SRLR is analyzed by both theoretical and parametric studies based on the even-/odd-mode method and EM full-wave simulations. It is found that the frequency separation of DMs and CMs can be enlarged by changing the admittance ratio K of the SI-SRLR, and a suitable value of the ratio can be determined for desired differential passbands and good CM suppression. To further suppress the transmission of CM signals, an open stub is loaded at the symmetric plane of SI-SRLR to misalign the two CM resonances without affecting the DM responses. Besides, a source-load coupling is introduced to produce multiple transmission zeros (TZs) at the two sides of both passbands and realize thereby high frequency selectivity. The analysis of SI-SRLR and the design details of the filter are given in sections II and III, respectively. The simulated and measured results of the filter show superior performance and are given in section IV.

II. ANALYSIS OF THE PROPOSED QUADRUPLE-MODE SI-SRLR

A. CONFIGURATION AND EQUIVALENT CIRCUIT OF SI-SRLR

The configuration of the proposed microstrip quadruple-mode SI-SRLR is depicted in Fig. 1. It consists of a one-wavelength stepped-impedance ring resonator loaded with two open-circuited stubs, which is different from the one-wavelength uniform-impedance ring resonator adopted in [21]–[23]. L_1 to L_3 and w_1 to w_4 denote the physical lengths and widths of the corresponding microstrip line segments,
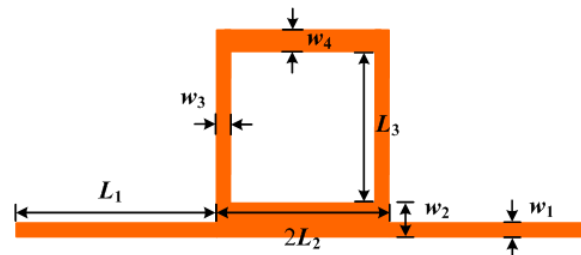

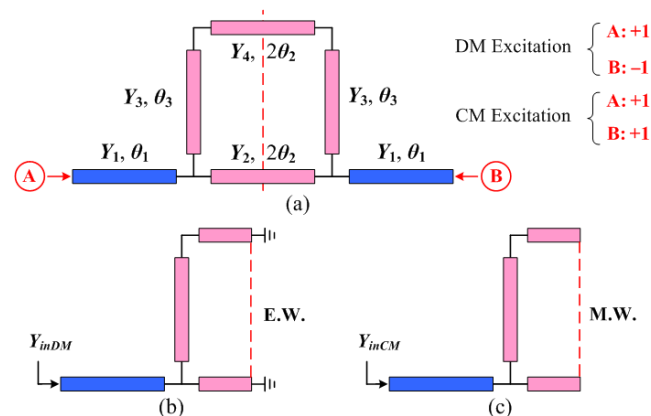**FIGURE 1.** Geometry of the proposed quadruple-mode SI-SRLR.

FIGURE 2. (a) Transmission line model of the proposed quadruple-mode SI-SRLR. (b) DM equivalent circuit. (b) CM equivalent circuit.

respectively. In light of the demonstrations in [23], the equivalent transmission line model (TLM) of the proposed SI-SRLR is also built for property analysis. TLM is shown in Fig. 2(a). This circuit consists of six transmission-line sections, with corresponding electrical lengths and characteristic admittances as θ_1, $2\theta_2$, θ_3, and Y_1, Y_2, Y_3, Y_4, respectively. Here, $\theta_1 = \beta L_1$, $\theta_2 = \beta L_2$, $\theta_3 = \beta L_3$, and β is the propagation constant of the microstrip line.

B. CHARACTERISTICS OF DM AND CM BISECTION

Since the circuit in Fig. 2(a) is a symmetric structure, it can be readily analyzed by using the well-known even- and odd-mode method, as conducted in [23]. In the case of even-mode excitation, the symmetrical plane of the circuit is an electrical wall (E.W.), and the circuit is simplified as shown in Fig. 2(b). For the odd-mode excitation, the symmetrical plane is a magnetic wall (M.W.), and the simplified circuit is given in Fig. 2(c).

The input admittance of the DM or CM equivalent circuit, $Y_{in,DM \text{ or } CM}$, can be derived as

$$Y_{in,\,DM\&CM} = Y_1 \frac{Y_L + jY_1 \tan\theta_1}{Y_1 + jY_L \tan\theta_1} \qquad (1)$$

where

$$Y_L = \begin{cases} jY_3 \dfrac{Y_3 \tan\theta_3 - Y_4 \cot\theta_2}{Y_3 + Y_4 \cot\theta_2 \tan\theta_3} - jY_2 \cot\theta_2, & DM\ case \\[3mm] jY_3 \dfrac{Y_3 \tan\theta_3 + Y_4 \tan\theta_2}{Y_3 - Y_4 \tan\theta_3 \tan\theta_2} + jY_2 \tan\theta_2, & CM\ case. \end{cases}$$
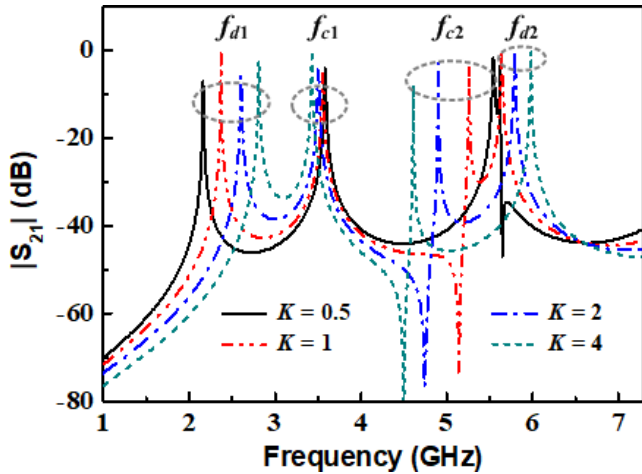$$(2)$$

FIGURE 3. Frequency responses of the SI-SRLR with different values of the admittance ratio *K*.

From the resonant condition of $Y_{in,DM \text{ or } CM} = 0$, the DM and CM resonant frequencies can be deduced as follows:

$$Y_3(Y_3 \tan\theta_3 - Y_4 \cot\theta_2) + (Y_1 \tan\theta_1 - Y_2 \cot\theta_2)$$
$$\times (Y_3 + Y_4 \tan\theta_3 \cot\theta_2) = 0, \quad DM \text{ case} \quad (3a)$$
$$Y_3(Y_3 \tan\theta_3 + Y_4 \tan\theta_2) + (Y_1 \tan\theta_1 + Y_2 \tan\theta_2)$$
$$\times (Y_3 - Y_4 \tan\theta_3 \tan\theta_2) = 0, \quad CM \text{ case.} \quad (3b)$$

For simplification, let $Y_1 = Y_3 = Y_4$, $\theta_1 = 2\theta_2$, and define $K = Y_2/Y_1$. Thus, (3) can be reformulated as

$$(\tan\theta_3 - \cot(\theta_1/2)) + (\tan\theta_1 - K\cot(\theta_1/2))$$
$$\times (1 + \tan\theta_3 \cot(\theta_1/2)) = 0, \quad DM \text{ case} \quad (4a)$$
$$(\tan\theta_3 + \tan(\theta_1/2)) + (\tan\theta_1 + K\tan(\theta_1/2))$$
$$\times (1 - \tan\theta_3 \tan(\theta_1/2)) = 0, \quad CM \text{ case.} \quad (4b)$$

It is obvious from (4) that both the DM resonant frequencies and the CM resonant frequencies can be varied by changing the electrical lengths θ_i ($i = 1, 2,$ and 3) and the admittance ratio *K*. The typical frequency responses of the SI-SRLR with different values of the admittance ratio *K* are drawn in Fig. 3, which are obtained by using the Agilent ADS simulator. In the simulation, θ_1 and θ_3 are chosen as 60° and 17°, respectively, at 2.2 GHz, and Y_1 is 0.01 S. It is seen from Fig. 3, four resonant modes of SI-SRLR are observed, including two DM modes at f_{d1} and f_{d2}, and two CM modes at f_{c1} and f_{c2}. As *K* increases, the frequencies of the two DM increase, while the two frequencies of CM reduce. We define $\Delta_1 = |f_{d1} - f_{c1}|$ and $\Delta_2 = |f_{d2} - f_{c2}|$, indicating the frequency separation between the two pairs of DM and CM modes. In Fig. 4, we show the variation of Δ_1 and Δ_2 against the admittance ration *K*. As can be seen, with the increase of *K*, Δ_1 decreases while Δ_2 increases. This means that the frequency separation between the two pairs of DM and CM modes can be adjusted by changing *K*.

In the design of differential BPF by using multimode resonator, DMs and CMs are always excited simultaneously.
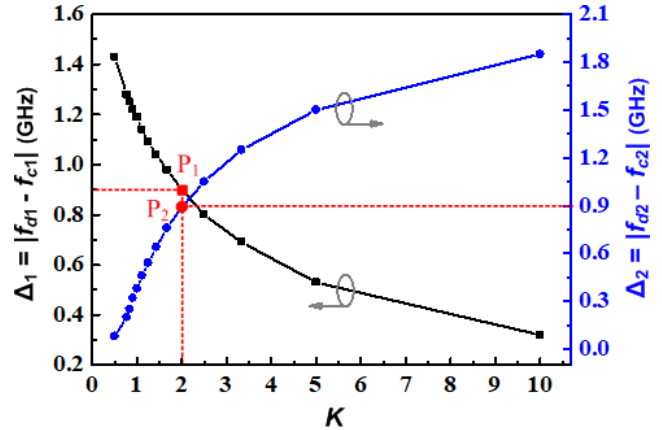

FIGURE 4. Variation of Δ 1 and Δ 2 with different admittance ratio K.
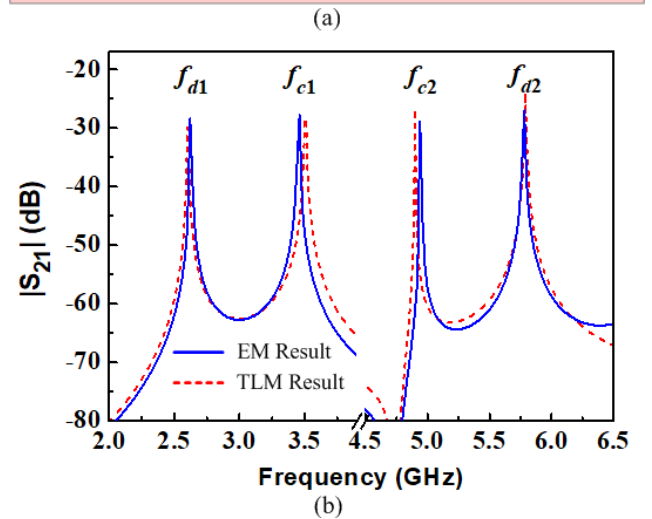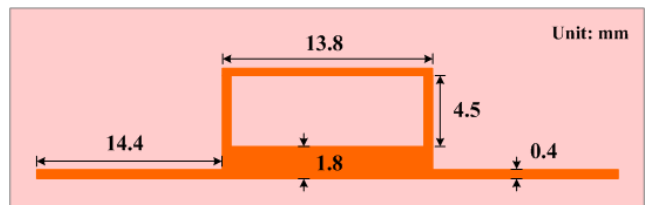

FIGURE 5. (a) Configuration of the designed quadruple-mode SI-SRLR. (b) EM and TLM simulated results of the SI-SRLR under weak excitations.

If the CM resonant frequency approaches close to the DM frequency, the CM will interfere with the DM, thereby degrading the performance of the differential system [9], [19]. Thus, a large frequency separation between two adjacent DM and CM is highly desired for good DM response and deep in-band CM suppression. As shown in Fig. 4, when a small *K* is chosen, we can get a big Δ_1 but Δ_2 is very small, and vice versa. When $K = 2$, a balanced frequency separation of the two pairs of DM and CM frequencies can be obtained. The corresponding Δ_1 and Δ_2 is 0.9 (|2.6 - 3.5|) GHz and 0.89 (|4.9 - 5.79|) GHz, respectively, as shown in Fig. 4. The simulated result of the SI-SRLR TLM by ADS simulator under weak excitation is portrayed the red dashed-line in Fig. 5(b).
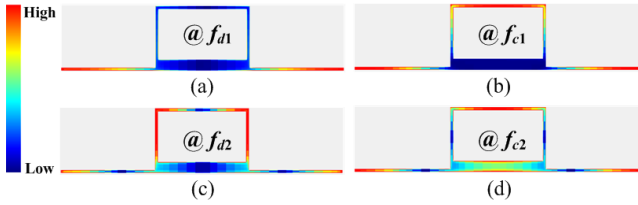
FIGURE 6. Simulated voltage distributions of SI-SRLR at four resonant modes. (a) f_{d1}. (b) f_{c1}. (c) f_{d2}. (d) f_{c2}.

III. DESIGN OF THE DUAL-BAND DIFFERENTIAL BPF

In this part, the SI-SRLR is employed to design a dual-band differential BPF with two passbands centered at 2.6 GHz and 5.8 GHz, respectively. Based on the analysis in section II, the dimensions of the quadruple-mode resonators are determined first. Next, the coupling between the feed line and the SI-SRLR and the coupling between two SI-SRLRs are investigated. At last, the source-load coupling method for producing TZs and the CM frequency dispersion technique for noise reduction are applied to improve the performance of both DM response and CM suppression.

A. DESIGN OF THE SI-SRLR

As concluded from Fig. 4, the admittance ration K of the SI-SRLR is chosen as 2 for obtaining the balanced frequency separation between the two pairs of DM and CM frequencies. separation between the two pairs of DM and CM frequencies. The other electrical parameters are kept the same as those used for Fig. 3, i.e., $\theta_1 = 60°$ and $\theta_3 = 17°$ at 2.2 GHz, and $Y_1 = 0.01$ S. Y_2 is then 0.02 S as $K = 2$ and $Y_1 = 0.01$ S. The substrate Taconic RF35 with a relative dielectric constant of 3.5 and a thickness of 0.8 mm is used in this paper. From the above electrical parameters, and by using the commercial electromagnetic software *Sonnet em*, the geometrical dimension of the SI-SRLR are obtained and are shown in Fig. 5(a). Its EM simulated frequency response under weak excitation is depicted as the blue solid line in Fig. 5(b). It can be obtained from figure that the simulated frequency separations Δ_1 and Δ_2 are 0.85 (|2.61 - 3.46|) GHz and 0.85 (|4.94 - 5.79|) GHz, respectively. The discrepancies of resonant frequencies and its separations between the EM simulation and the TLM calculation are attributed to the parasitic effects in EM modeling, which are ignored in the TLM. Fig. 6 exhibits the simulated voltage distribution over the SI-SRLR at four resonant modes. It is observed that the voltage is mainly concentrated on two open-circuited stubs at f_{d1} whereas the voltage distributes on not only the one part of the open-circuited stubs but also the vertical segments of square ring at f_{d2}. For CM resonances, the voltage distributions cover the open-circuited stubs as well as the horizontal segments of square ring. The discrepancy of voltage distributions between the DM and CM resonances is advantage for CM suppression by using the auxiliary method.

B. DESIGN OF THE DUAL-BAND DIFFERENTIAL BPF

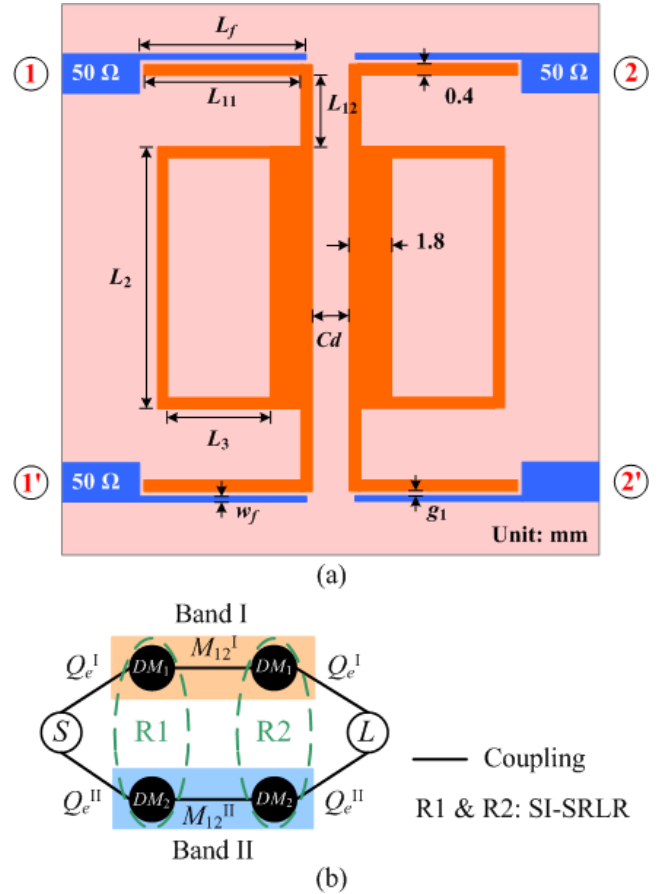In this part, a second-order dual-band differential BPF is designed based on the previous design of the

FIGURE 7. (a) Configuration of the dual-band differential BPF. (b) Coupling scheme of the BPF under DM operation.

quadruple-mode SI-SRLR. Fig. 7(a) presents the geometrical structure of the designed dual-band differential BPF with two coupled SI-SRLRs. For size reduction, the open-stubs of the SI-SRLR are folded. The two passbands having Chebyshev response with 0.04321-dB ripple level are specified at 2.6 GHz and 5.8 GHz. The corresponding desired fractional bandwidth (FBW) is 4.12% and 1.5%, respectively. The coupling scheme of the BPF under DM operation is depicted in Fig. 7(b), where nodes S and L denote input and output ports, respectively. Nodes DM_1 and DM_2 represent the two DMs of SI-SRLR at fd_1 and fd_2. There are two coupling paths, each coupling path forms a DM passband. The lumped circuit elements of the low-pass prototype filter are found to be $g_0 = 1$, $g_1 = 0.6648$, $g_2 = 0.5445$, and $g_3 = 1.2210$ [24]. Based on (5) and (6), the required coupling parameters shown in Fig. 7(b) are: the coupling coefficients $M_{12}^{I} = 0.0684$ and $M_{12}^{II} = 0.0249$, the external quality factors $Q_e^{I} = 16.2$ and $Q_e^{II} = 44.3$.

$$M_{i,i+1} = \frac{FBW}{\sqrt{g_i g_{i+1}}} \quad \text{for } i = 1 \text{ to } n-1 \quad (5)$$

$$Q_e = \frac{g_0 g_1}{FBW} \quad (6)$$

From the above external Q values and coupling coefficients, we determine the dimensions of both the feed
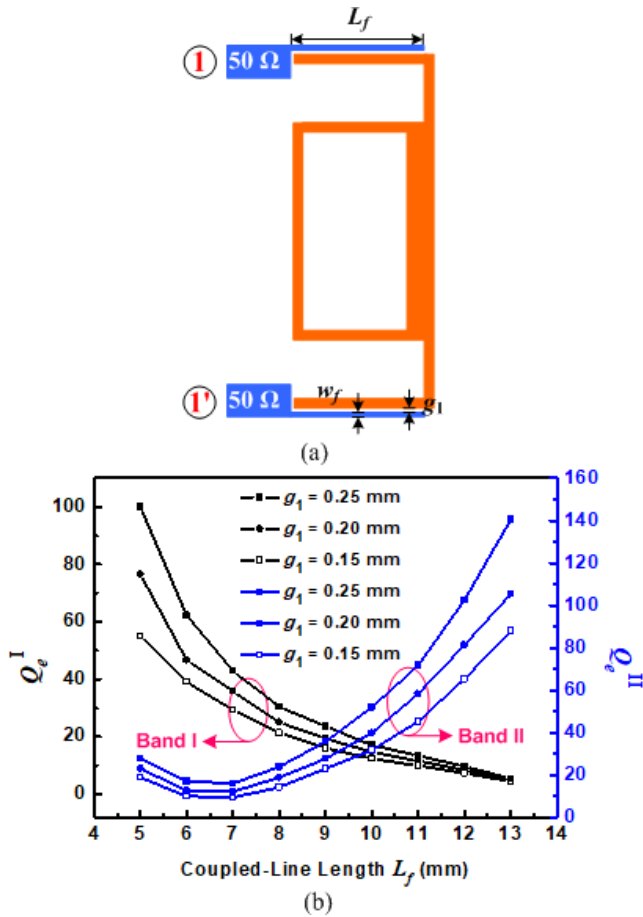
FIGURE 8. (a) Parallel-coupled feed line structure of SI-SRLR. (b) The extracted Q_e for two passbands under DM excitation, where $w_f = 0.2$ mm.

FIGURE 9. (a) Configuration of two coupled SI-SRLRs. (b) Coupling coefficients as a function of the coupling space C_d under DM excitation.

line structure and the internal coupling space between two SI-SRLRs, using the simulator Sonnet em. As shown in Fig. 8(a), microstrip parallel-coupled lines are chosen as the feeding structure in this design. The line width and coupling gap are denoted as w_f and g_1, respectively. Fig. 8(b) plots the computed variation of the external Q values, Q_e^I for the first passband and Q_e^{II} for the second passband, versus the coupled-line length L_f when $w_f = 0.2$ mm. Note that a strong I/O coupling leads to a small external quality factor of a resonator [24]. So, it is seen that Q_e^I decreases monotonously as L_f increases. While for Q_e^{II}, it decreases at first as L_f increases when L_f is smaller than 7 but then increases monotonously when L_f is larger than 7. The difference of the variations for two Q_e is attributed to the different voltage distributions of two DM resonances on the open-circuited stubs, as indicated in Fig. 6. Also, it can be observed that as the coupling gap g_1 increases, the external Q values of both passbands becomes larger. Because a larger coupling gap results in a weaker I/O coupling. From Fig. 8(b), the L_f and g_1 are determined as 9.3 mm and 0.2 mm, respectively, for the designed filter.

Figure 9(a) shows the configuration of two coupled SI-SRLRs, in which C_d and L_{12} are the coupling distance and length to adjust the total coupling strength. It should be noted
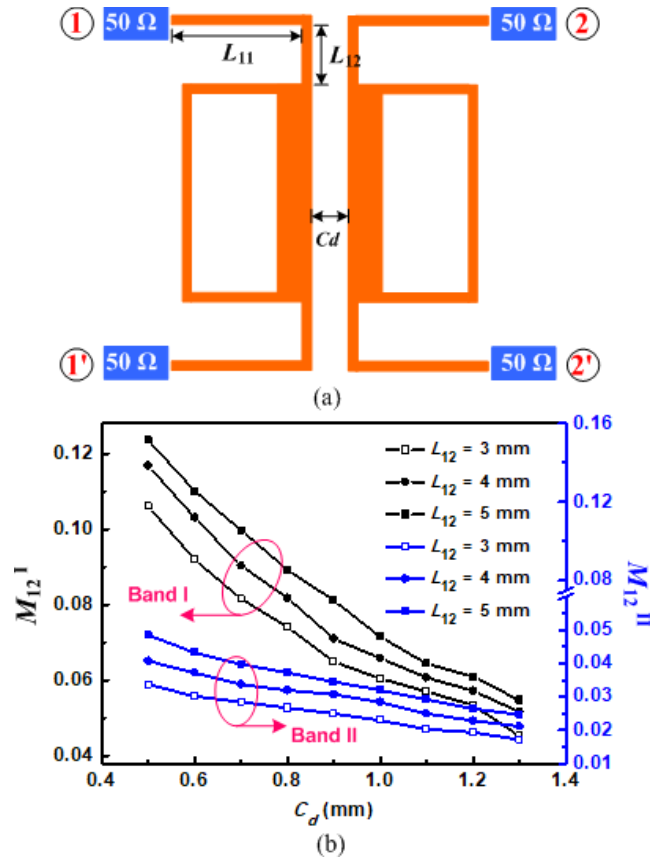
that the sum of L_{11} and L_{12} should be remained a constant in order to keep the resonant frequency unchanged. Fig. 9(b) provides the computed variation of coupling coefficients, M_{12}^I for passband I and M_{12}^{II} for passband II, versus the coupling space C_d. It can be seen that the coupling coefficients of both passbands decrease monotonously as C_d increases or L_{12} decreases. From Fig. 9(b), the C_d and L_{12} are determined as 0.9 mm and 4 mm, respectively, for the designed filter. The remained geometrical dimensions in Fig. 7(a) are obtained after optimizing the frequency response of the filter using Sonnet, and these are: $L_{11} = 8.7$ mm, $L_2 = 13.8$ mm and $L_3 = 6.1$ mm. With these geometrical parameters, the frequency response of designed dual-band differential BPF is simulated and depicted in Fig. 10. The simulated two DM passbands are centered at 2.6 and 5.8 GHz, and their corresponding FBW is 4.13% and 1.51%, respectively, which agree well with the desired specifications. Two reflection zeros are observed in both passbands and the return losses are better than 20 dB. The insertion losses of two passbands are 0.2 dB and 0.5 dB, which are mainly attributed to the dielectric loss (loss tangent is 0.0018).

In view of the CM response, it is seen that the minimum CM suppression is 40 dB within the first DM passband and 15 dB within the second DM passband. Besides, there is a CM resonance peak between the two passbands. Therefore,
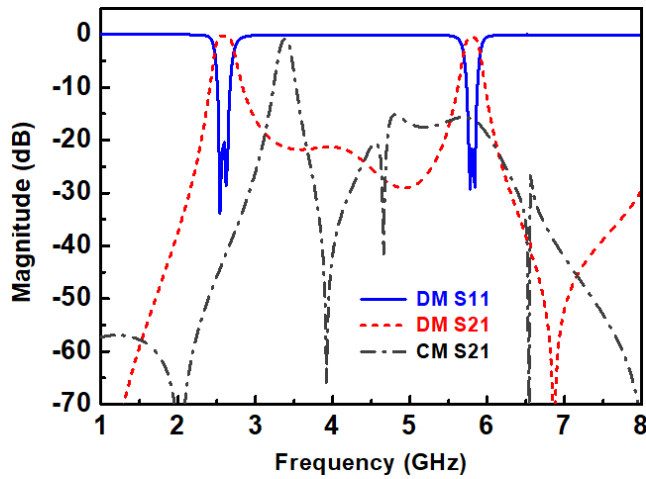
**FIGURE 10.** Simulated DM &CM responses of the dual-band differential BPF.

the CM suppression should be increased. In addition, improvement of the selectivity of the two DM passbands is also wanted.

As shown in Fig. 7(a), the differential BPF has two identical SI-SRLRs, which have thereby identical DM and CM resonances. As a result, when DM resonances are well coupled to form the desired differential passbands, the CM noise will also be transmitted from the input to output by the built CM coupling path, thus incurring poor CM rejection.

As studied in [6] and [12], the frequency discrepancy technique by separating the CM resonances in adjacent resonators is an effective method to block the transmission of CM signals. As illustrated in Fig. 6, it is obtained that the voltage on the center segment of resonator at two DMs are both near to null, while the voltage at CMs are strong, especially on the high-impedance line segment. Therefore, the CM resonances will be shifted by inserting loaded elements at the symmetric plane while the DM resonances will be affected little. As shown in Fig. 11(a), an open stub with a length S_L and a width S_w is loaded at the center of the left SI-SRLR to shift its CM resonances. Then, the CM coupling between the left and right SI-SRLRs will be weaken, and the CM transmission will be reduced.

To enhance further the CM suppression within the DM passbands and improve the selectively of DM passbands, two short microstrip lines with a length L_{SL} and a width w_{SL} are added closely to the input and output feed lines, as shown in Fig. 11(a). Fig. 11(b) depicts the coupling scheme of the improved filter under DM excitation. Compared with the coupling scheme in Fig. 7(b), the coupling M_{SL} between the source and load is introduced, which provides an additional transmission path. Based on the theory of transversal signal interference, multiple TZs will be produced and improve thereby the frequency selectivity of the BPF [23].

In addition, the introduced source-load coupling has also influence on the CM response as it changes the locations of TZs or produces new TZs under CM condition. With appropriate choice of the coupling strength, the CM TZs can be
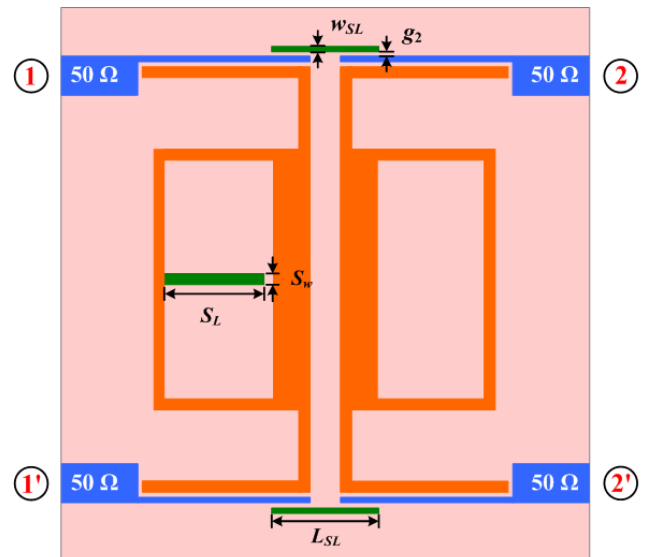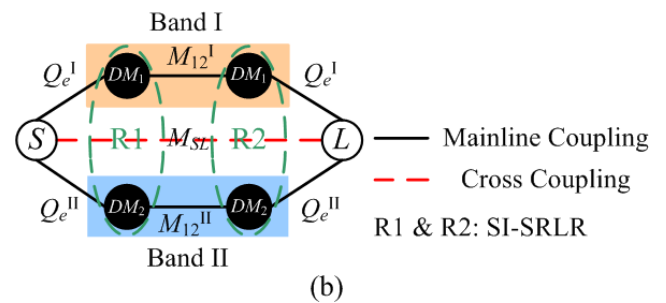
FIGURE 11. (a) Configuration of the improved dual-band differential BPF. (b) Coupling scheme of the improved BPF under DM condition.

tuned to or produced at frequencies within the DM passbands, which will enhance significantly the CM rejection in the DM passbands. The parameterization and optimization tools of *Sonnet* are utilized to speed up the design process. After fine tuning, the dimensions for the loaded stub and the source-load coupling lines are finally determined as follows: $S_L = 5.9$, $S_w = 0.4$, $L_{SL} = 5.1$, $w_{SL} = 0.2$, and $g_2 = 0.25$ (unit: mm).

IV. MEASURED RESULTS OF THE DIFFERENTIAL BPF

To verify the above design and the performance of the filter, the circuit shown in Fig. 11(a) is fabricated, and its photograph is shown in Fig. 12. The overall size (excluding the feed lines) is 18.2 mm × 24.0 mm, about $0.26 \lambda_g \times 0.34\lambda_g$, where λ_g is the guide wavelength at 2.6 GHz. The filter measurement is executed on a four-port vector network analyzer, Agilent E5071C.

In Fig. 13 the simulated DM response is drawn by blue solid lines. Apparently, four DM TZs, located at 1.9 GHz, 3.78 GHz, 5.3 GHz, and 6.15 GHz, are located in the vicinities of the passbands, which highly improve the selectivity of two DM passbands. The simulated CM response is depicted in red solid line. It is observed that the minimum CM suppression within the DM passband are 60 dB for the first passband and 45 dB for the second passband.

TABLE 1. Comparison of some previous dual-band differential/balanced filters.

Ref.	Center Frequency (GHz)	3-dB FBW (%)	Line type of Resonators	Insertion Loss (dB)	CM Attenuation in Two DM Passbands (dB)	Number of TZs	Circuit Size ($\lambda_g \times \lambda_g$)
[5]	2.45 / 5.25	9.8 / 4.6	Microstrip	2.4 / 2.82	53 / 45	0	0.38 × 0.42
[6]	2.46 / 5.56	16.3 / 6.7	Microstrip & Lumped Elements	1.9 / 1.9	36 / 31	4	0.31 × 0.41
[7]	2.5 / 5.6	N/A	Microstrip & DGS	1.29 / 1.97	34.7 / 24.1	1	0.15 × 0.27
[9]	2.5 / 5.8	12.9 / 4.5	Microstrip	0.77 / 1.56	42 / 38	0	0.15 × 0.37
[10]	1.8 / 5.8	4.5 / 1.8	Microstrip	1. 2 / 2.0	35 / 25	4	0.37 × 0.28
[11]	2.4 / 3.57	7.5 / 5.0	Microstrip	0.87 / 1.9	28 / 31	1	0.50 × 0.20
[12]	2.4 /5	16.4 / 8.6	Microstrip	1.78 / 2.53	32 / 32	1	0.50 × 0.70
[13]	2.44 / 5.19	18 / 8.7	Microstrip & Slotline	1.14 / 2.05	42 / 42	3	N/A
[14]	2.64 / 5.17	24.6 / 13.9	Microstrip & Slotline	0.88 / 1.51	65 / 52	2	N/A
[15]	2.45 / 5.85	6.5 / 3.0	Microstrip & Lumped Elements	1.06 / 2.04	25 / 25	1	N/A
[16]	0.9 / 2.49	3.6 / 2.1	Microstrip	2.67 / 4.65	30 / 40	3	0.53 × 1.10
[17]	9.47 / 9.96	2.9 / 3.1	SIW	1.89 / 1.73	30 / 30	1	2.87 × 2.95
[18]	9.23 / 14.05	2.8 / 5.6	SIW & Slotline	2.9 / 2.7	48 / 40	N/A	2.70 × 1.27
[20]	3.58 / 5.6	5.8 / 3.4	Microstrip	1.1 / 1.8	25 / 17	4	0.25 × 0.47
This work	**2.6 / 5.8**	**10.4 / 3.6**	**Microstrip**	**1.1 / 2.15**	**62 / 48**	**4**	**0.26 × 0.34**
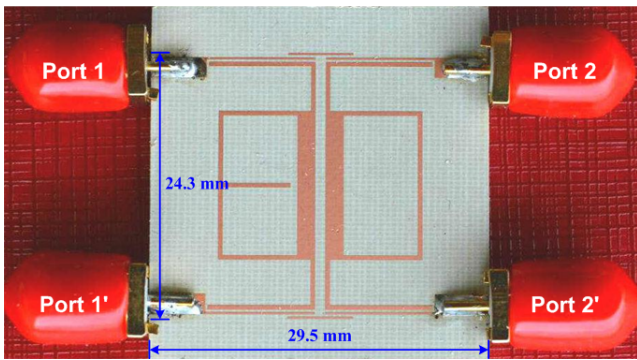
FIGURE 12. Photograph of the fabricated dual-band differential BPF.

FIGURE 13. Simulated and measured frequency responses of the BPF.

The dashed lines in Fig. 13 represent the measured responses of the filter, which agree reasonably with the simulated data. For the DM responses, the measured first and second passbands are centered at 2.58 and 5.79 GHz, respectively, with corresponding 3-dB frequency ranges of 2.44 - 2.71 GHz and 5.68 - 5.89 GHz. The measured minimum insertion losses are 1.1 dB and 2.1 dB for the first and the second passband, respectively. Four TZs, located at 1.8 GHz, 3.77 GHz, 5.3 GHz, and 6.17 GHz, are observed and improve significantly the passband selectivity. For CM response, the measured minimum CM insertion losses within the DM passbands are 62 dB for the first passband and 48 dB for the second passband, which show a good CM suppression level within DM passbands. Besides, CM suppression over 1 to 8 GHz is better than 15 dB. Deviations between the simulated and measured results are mainly due to the fabrication tolerance and the parasitic effects from
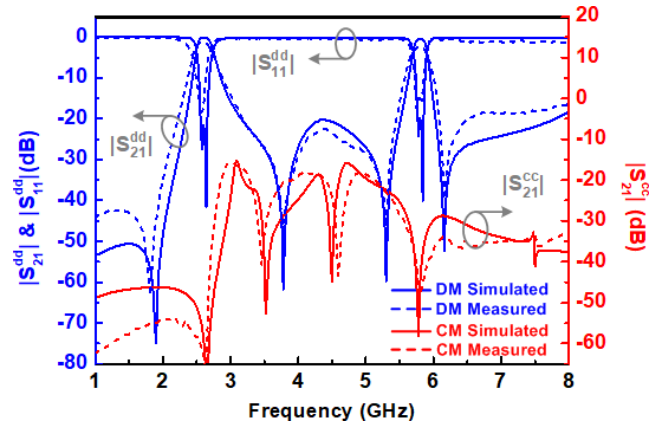
the solder connections. Moreover, the comparison of proposed dual-band filter with other differential dual-band filters is summarized in Table 1. It is seen that the proposed differential filter outperforms the works in [7] and [9] in terms of the CM rejection and the selectivity of DM passbands. Also, the circuit size is found to be competitive when compared with the other designs.

V. CONCLUSION

In this paper, a novel dual-band differential BPF is developed based on the proposed quadruple-mode SI-SRLR. DM and CM characteristics of the SI-SRLR are analyzed by the even- and odd-mode method. The admittance ratio K of SI-SRLR is used to obtain balanced frequency separations of two pairs of DM and CM resonances, which is important to prevent the

interference between DM and CM resonances. Furthermore, stub-loading and source-load coupling techniques are applied to improve the CM suppression in a wide frequency range and enhance the frequency selectivity of DM passbands. The designed dual-band differential BPF has the advantages of small size, high performance DM passbands, and large CM suppression over a wide frequency range, which are attractive in the applications for differential multimode and multiband communication systems.

REFERENCES

[1] Y. Wu, L. Cui, W. Zhang, L. Jiao, Z. Zhuang, and Y. Liu, "High performance single-ended wideband and balanced bandpass filters loaded with stepped-impedance stubs," *IEEE Access*, vol. 5, pp. 5972–5981, Apr. 2017.

[2] C.-H. Wu, C.-H. Wang, and C. H. Chen, "Novel balanced coupled-line bandpass filters with common-mode noise suppression," *IEEE Trans. Microw. Theory Techn.*, vol. 55, no. 2, pp. 287–295, Feb. 2007.

[3] C.-H. Wu, C.-H. Wang, and C. H. Chen, "Stopband-extended balanced bandpass filter using coupled stepped-impedance resonators," *IEEE Microw. Wireless Compon. Lett.*, vol. 17, no. 7, pp. 507–509, Jul. 2007.

[4] C.-H. Wu, C.-H. Wang, and C. H. Chen, "Balanced coupled-resonator bandpass filters using multisection resonators for common-mode suppression and stopband extension," *IEEE Trans. Microw. Theory Techn.*, vol. 55, no. 8, pp. 1756–1763, Aug. 2007.

[5] C.-H. Lee, C.-I. G. Hsu, and C.-C. Hsu, "Balanced dual-band BPF with stub-loaded SIRs for common-mode suppression," *IEEE Microw. Wireless Compon. Lett.*, vol. 20, no. 2, pp. 70–72, Feb. 2010.

[6] J. Shi and Q. Xue, "Dual-band and wide-stopband single-band balanced bandpass filters with high selectivity and common-mode suppression," *IEEE Trans. Microw. Theory Techn.*, vol. 58, no. 8, pp. 2204–2212, Aug. 2010.

[7] J. X. Chen, M.-Z. Du, Y.-L. Li, Y.-J. Yang, and J. Shi, "Independently tunable/controllable differential dual-band bandpass filters using element-loaded stepped-impedance resonators," *IEEE Trans. Compon. Packag. Manuf. Technol.*, vol. 8, no. 1, pp. 113–120, Jan. 2018.

[8] J. Shi and Q. Xue, "Balanced bandpass filters using center-loaded half-wavelength resonators," *IEEE Trans. Microw. Theory Techn.*, vol. 58, no. 4, pp. 970–977, Apr. 2010.

[9] F. Wei, Y. J. Guo, P. Y. Qin, and X. W. Shi, "Compact balanced dual- and tri-band bandpass filters based on stub loaded resonators," *IEEE Microw. Wireless Compon. Lett.*, vol. 25, no. 2, pp. 76–78, Feb. 2015.

[10] X. Wu, F. Wan, and J. Ge, "Stub-loaded theory and its application to balanced dual-band bandpass filter design," *IEEE Microw. Wireless Compon. Lett.*, vol. 26, no. 4, pp. 231–233, Apr. 2016.

[11] Y.-H. Cho and S.-W. Yun, "Design of balanced dual-band bandpass filters using asymmetrical coupled lines," *IEEE Trans. Microw. Theory Techn.*, vol. 61, no. 8, pp. 2814–2820, Aug. 2013.

[12] J. Shi and Q. Xue, "Novel balanced dual-band bandpass filter using coupled stepped-impedance resonators," *IEEE Microw. Wireless Compon. Lett.*, vol. 20, no. 1, pp. 19–21, Jan. 2010.

[13] X. Guo, L. Zhu, and W. Wu, "Balanced wideband/dual-band BPFs on a hybrid multimode resonator with intrinsic common-mode rejection," *IEEE Trans. Microw. Theory Techn.*, vol. 64, no. 7, pp. 1997–2005, Jul. 2016.

[14] X. Guo, L. Zhu, and W. Wu, "A dual-wideband differential filter on strip-loaded slotline resonators with enhanced coupling scheme," *IEEE Microw. Wireless Compon. Lett.*, vol. 26, no. 11, pp. 882–884, Nov. 2016.

[15] F. Bagci, A. Fernández-Prieto, A. Lujambio, J. Martel, J. Bernal, and F. Medina, "Compact balanced dual-band bandpass filter based on modified coupled-embedded resonators," *IEEE Microw. Wireless Compon. Lett.*, vol. 27, no. 1, pp. 31–33, Jan. 2017.

[16] L. Yang, W.-W. Choi, K.-W. Tam, and L. Zhu, "Balanced dual-band bandpass filter with multiple transmission zeros using doubly short-ended resonator coupled line," *IEEE Trans. Microw. Theory Techn.*, vol. 63, no. 7, pp. 2225–2232, Jul. 2015.

[17] X. Xu, J. Wang, G. Zhang, and J. Chen, "Design of balanced dual-band bandpass filter based on substrate integrated waveguide," *Electron. Lett.*, vol. 49, no. 20, pp. 1278–1280, Sep. 2013.

[18] Y. Shen, H. Wang, W. Kang, and W. Wu, "Dual-band SIW differential bandpass filter with improved common-mode suppression," *IEEE Microw. Wireless Compon. Lett.*, vol. 25, no. 2, pp. 100–102, Feb. 2015.

[19] L.-H. Zhou, Y.-L. Ma, J. Shi, J.-X. Chen, and W. Q. Che, "Differential dual-band bandpass filter with tunable lower band using embedded DGS unit for common-mode suppression," *IEEE Trans. Microw. Theory Techn.*, vol. 64, no. 12, pp. 4183–4191, Dec. 2016.

[20] L.-H. Zhou and J.-X. Chen, "Differential dual-band filters with flexible frequency ratio using asymmetrical shunt branches for wideband CM suppression," *IEEE Trans. Microw. Theory Techn.*, vol. 65, no. 11, pp. 4606–4615, Nov. 2017.

[21] H. Liu, B. Ren, X. Guan, J. Lei, and S. Li, "Compact dual-band bandpass filter using quadruple-mode square ring loaded resonator (SRLR)," *IEEE Microw. Wireless Compon. Lett.*, vol. 23, no. 4, pp. 181–183, Apr. 2013.

[22] T. Du, B. Guan, A. Wu, and Z. Zhang, "Dual-band bandpass filter based on quadruple-mode open stub loaded square ring resonator," in *Proc. IEEE Int. Conf. Signal Process., Commun. Comput. (ICSPCC)*, Xiamen, China, Oct. 2017, pp. 1–4.

[23] H. Liu, B. Ren, X. Guan, P. Wen, and Y. Wang, "Quad-band high-temperature superconducting bandpass filter using quadruple-mode square ring loaded resonator," *IEEE Trans. Microw. Theory Techn.*, vol. 62, no. 12, pp. 2931–2941, Dec. 2014.

[24] J.-S. Hong and M. J. Lancaster, *Microstrip Filters for RF/Microwave Applications*. New York, NY, USA: Wiley, 2001.

BAOPING REN (S'16) received the B.S. degree in communication engineering and the M.S. degree in communication and information system from East China Jiaotong University, Nanchang, China, in 2011 and 2014, respectively. He is currently pursuing the Ph.D. degree in microwave engineering with Saitama University, Japan. In 2014, he became a Research Assistant with East China Jiaotong University. His current research interests include microwave circuits and devices, and high-temperature superconducting filters.

HAIWEN LIU (M'04–SM'13) received the B.S. degree in electronic system and the M.S. degree in radio physics from Wuhan University, Wuhan, China, in1997 and 2000, respectively, and the Ph.D. degree in microwave engineering from Shanghai Jiao Tong University, Shanghai, China, in 2004. From 2004 to 2006, he was with Waseda University, Kitakyushu, Japan, as a Research Assistant Professor. From 2006 to 2007, he was a Research Fellow with the University of Kiel, Kiel, Germany, where he was a recipient of the Alexandervon Humboldt Research Fellowship. From 2007 to 2008, he was a Professor with the Institute of Optics and Electronics, Chengdu, China, where he was supported by the 100 Talents Program of the Chinese Academy of Sciences. From 2009 to 2017, he was a Chair Professor with East China Jiaotong University, Nanchang, China. He is currently a Full Professor with Xi'an Jiaotong University, Xi'an, China. He has published over 100 papers in international and domestic journals and conferences. His current research interests include the electromagnetic modeling of high-temperature superconducting circuits, radio frequency and microwave passive circuits and systems, antennas theory, and radar systems.

Dr. Liu has served as a technical program committee member for many international conferences. He was a recipient of the Wang Kuancheng Science Foundation in 2008, the Best Paper Prize of the 2005 International Conference on Communications, Circuits and Systems Proceedings, Hong Kong, the Prize of Osaka City Mayor for the Conference of Chinese Alumni in Japan in 2005, and the 100 Best Ph.D. Dissertations in Shanghai, China, in 2006. He was a Reviewer of some international journals, including the IEEE Transactions on Microwave Theory and Technique, the IEEE Transactions on Applied Superconductivity, the IEEE Transactions on Industrial Electronics, the IEEE Microwave and Wireless Components Letters, and the IEEE Antennas and Wireless Propagation Letters.

ZHEWANG MA (M'96) received the B.Eng. and M.Eng. degrees from the University of Science and Technology of China, Hefei, China, in 1986 and 1989, respectively, and the Dr.-Eng. degree from the University of Electro-Communications, Tokyo, Japan, in 1995.

In 1996, he was a Research Assistant with the Department of Electronic Engineering, University of Electro-Communications, where he became an Associate Professor in 1997. From 1998 to 2008, he was an Associate Professor with the Department of Electrical and Electronic Systems, Saitama University, where he became a Professor in 2009. His current research interests include the development of microwave and millimeter-wave devices and circuits, measurements of dielectric materials, and high-temperature superconductors. He is a member of the Review Board of the *IEICE Transactions on Electronics*.

Dr. Ma was a member of the Steering and/or Technical Committees of the 2002, 2006, and 2010 Asia-Pacific Microwave Conference. He is a Senior Member of the Institute of Electronics, Information and Communication Engineers (IEICE), Japan. He is the Vice President of the Technical Group on Electronics Simulation Technology, Electronics Society, IEICE. He was a recipient of the Japanese Government Graduate Scholarship from 1991 to 1993 and the URSI Young Scientist Award in 1993. From 1994 to 1996, he was a Research Fellow of the Japan Society for the Promotion of Science. He has served on the Editorial Board of the IEEE TRANSACTIONS ON MICROWAVE THEORY AND TECHNIQUES and the Review Board of the IEEE MICROWAVE AND WIRELESS COMPONENTS LETTERS.

MASATAKA OHIRA (M'06) received the B.E., M.E., and D.E. degrees from Doshisha University, Kyoto, Japan, in 2001, 2003, and 2006, respectively. From 2006 to 2010, he was with ATR Wave Engineering Laboratories, Kyoto, where he was involved in the research and development of small smart antennas, millimeter-wave circuits, and antennas for wireless communications. In 2010, he joined Saitama University, Saitama, Japan, where he is currently an Associate Professor. His current research interests include with the analysis and design of microwave and millimeter-wave filters and antennas.

Dr. Ohira is a member of the Institute of Electronics, Information and Communication Engineers (IEICE), Japan, the Institute of Electrical Engineers, Japan, and the European Microwave Association. He was a recipient of the IEICE Young Engineer Award in 2005 and the IEEE AP-S Japan Chapter Young Engineer Award in 2012. He was the Chair of the IEEE Microwave Theory and Techniques Society Kansai Chapter Young Engineers' Committee for 2008–2009.

PIN WEN received the B.S. degree in communication engineering and M.S. degree in communication and information system from East China Jiaotong University, Nanchang, China, in 2012 and 2015, respectively. He is currently pursuing the Ph.D. degree in microwave engineering with Saitama University, Japan.

In 2015, he became a Research Assistant with East China Jiaotong University. His current research interests include antenna theory and design, and superconducting filter design.

XIAOLONG WANG (M'12) received the B.S. degree in communication engineering from Jilin University, Changchun, China, in 2005, the M.S. degree from the Changchun University of Science and Technology, Changchun, in 2008, and the Ph.D. degree from the University of Toyama, Toyama, Japan, in 2012.

From 2012 to 2013, he was with the Art, Science and Technology Center for Cooperative Research, Kyushu University, Fukuoka, Japan, as a Post-Doctoral Research Associate. Since 2013, he has been with the Plasma Research Center, University of Tsukuba, Ibaraki, Japan. From 2016 to 2018, he was an Assistant Professor with Saitama University, Japan. He is currently a Full Professor with Jilin University. His research interests include microwave/millimeter-wave system design, passive component design, and optimization techniques.

Dr. Wang is a member of the Institute of Electronics, Information and Communication Engineers, Japan. He was a recipient of the IEEE Microwave Theory and Techniques Society Japan Chapter Young Engineer Award in 2013.

XUEHUI GUAN (M'11) received the B.S. degree in communication engineering from Jiangxi Normal University, Nanchang, China, in 1988, and the Ph.D. degree in electromagnetic fields and microwave techniques from Shanghai University, Shanghai, China, in 2007.

In 2012, he was a Senior Researcher Associate with the School of Electrical and Electronic Engineering, City University of Hong Kong, Hong Kong. Since 2013, he has been a Visiting Scholar with the School of Electrical and Electronic Engineering, Nanyang Technological University, Singapore. In 2016, he became a Professor with East China Jiaotong University, Nanchang. His current research interests include radio frequency and microwave passive circuits and system, synthesis theory and realization of microwave filters, and antennas for wireless communications.

• • •